Direct Observation of s-Wave Atomic Collisions

Kurt Gibble, Seongsik Chang, and Ronald Legere
Department of Physics, Yale University, New Haven, Connecticut 06520-8120
(Received 23 June 1995)

We observe the angular distribution of s-wave scattering of Cs atoms in an atomic fountain by selecting and probing atomic velocities. At an average temperature of $T = 0.89\ \mu$K the scattering is predominantly s-wave and we have a sensitivity to p-wave cross sections as small as 0.1% of the s-wave. The cross section is 4×10^{-11} cm^2 for atoms in the $F = 3$, $m_F = 0$ state colliding with atoms distributed among the $F = 4$, m_F states. We also demonstrate a multiply loaded magneto-optic trap and a temperature of 1.53(7) μK.

PACS numbers: 34.50.–s, 42.50.Vk, 32.80.Pj

At μK temperatures, quantum effects lead to novel phenomena in atom-atom interactions. These include quantum collective behaviors such as Bose-Einstein condensation, other indistinguishable particle effects, and cross sections as large as 10^6 Å^2. The potentially large cross sections occur because the de Broglie wavelength of the atom is much larger than the range of the interatomic potential. For Cs, $\lambda_{\mathrm{dB}} = 3000$ Å at 1 μK. Therefore only s-wave scattering is expected and cross sections may be as large as $\lambda_{\mathrm{dB}}^2/\pi$ [1]. These ultracold collisions play an important role in recent attempts to achieve Bose condensation by evaporative cooling in a trap [2] and also produce large frequency shifts imposing limitations on precision measurements using cold atoms [3–5].

Ultracold atom-atom collisions have previously been observed using four techniques: thermalization of atoms in a trap [2], cryogenic He beams [6], cryogenic H masers and their precursors [7], and frequency shifts in a laser-cooled Cs fountain clock [5]. All of these techniques are primarily sensitive to the total collision cross section and not to the angular distribution of the scattering. Here we observe the angular distribution of s-wave atomic scattering for the first time. We also demonstrate a multiply loaded magneto-optic trap (MOT) and low temperatures in a Cs fountain.

We begin with a sample of atoms at 1.5 μK. We then select a narrow velocity class by transferring atoms from one ground state sublevel to another using the Doppler shift on a two-photon (Raman) transition [8]. The selected atoms collide, which redistributes their velocities. By probing the resulting distribution, we observe the effects of collisions.

The measured velocity distribution is sensitive to the angular distribution of the scattering. This is most clearly illustrated when the selected velocity v_z' is much greater than the most probable thermal speed $u = (2kT/m)^{1/2}$. Here the velocity change after a single collision is $\frac{1}{2}\, v_z'[\cos(\theta) - 1]$, where θ is the center-of-mass scattering angle. When $v_z' \not\gg u$, the expression for the velocity change is not so simple because the Doppler shift only selects and probes one component of the atom's velocity. Therefore we must integrate over the initial and final transverse velocities of the detected atom and over all the velocity components of the atom with which it collides. This velocity redistribution is characterized by the velocity-changing collision kernel $W(v_z' \rightarrow v_z)$ [9].

A schematic of the vacuum chamber for our multiply loaded magneto-optic trap (MOT) is shown in Fig. 1. In the "vapor cell MOT," slow atoms in the room temperature Cs gas are slowed and trapped [10]. These atoms are then launched upwards by cooling into a moving frame [8]. The atoms are captured by the "UHV MOT" in Fig. 1. To multiply load [11], the vapor cell MOT is loaded again and more atoms are launched into the UHV MOT. The vapor cell MOT has a trap lifetime of 100 to 200 ms and, in this experiment, cold atoms are loaded for 46 ms and launched into the UHV MOT every 50 ms. During the launch the detuning of the downward propagating laser beams is -16 MHz and the atoms are accelerated to 10 m/s before leaving the laser beams. By multiply loading a trap in ultrahigh vacuum, we have a high loading rate and a long lifetime. We have

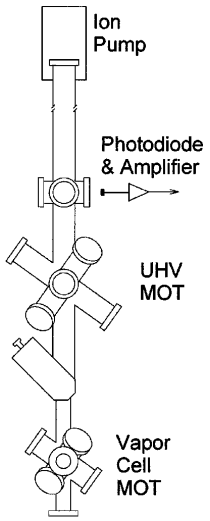

FIG. 1. Schematic of double magneto-optic trap (MOT) and fountain. Atoms are captured from Cs vapor in the "vapor cell MOT" and launched into the "UHV MOT." For scale, the window diameter is 5.1 cm [17]. The bias magnetic field and the Raman, "clearing," and "detection" laser beams are perpendicular to the plane of the figure.

 0031-9007/95/75(14)/2666(4)$06.00

demonstrated the loading of 6×10^{10} Cs atoms with a loading time constant of 0.65 s in the UHV MOT and a decay lifetime of 1.3 s after the loading ceases. For the data reported here, 6×10^9 atoms were loaded in 0.472 s.

Our atomic fountain is realized by accumulating atoms in the UHV MOT and launching them. To launch, the frequency of the three upward propagating laser beams of the UHV MOT is shifted by +2.656 MHz, giving the atoms a vertical velocity of 1.95 m/s. After 0.5 ms the Ti:sapphire laser frequency is shifted to allow cooling to low temperatures [12]. The detuning of the trapping beams from the Cs $6S$, $F = 4$ to $6P_{3/2}$, $F = 5$ transition is swept from -18 to ≈ -70 MHz. After another 1.5 ms, the intensity of the laser beams is ramped to $\frac{1}{16}$ of the trapping intensity, held for 1 ms, and then taken to zero in 0.4 ms. This is achieved by double passing two acousto-optic modulators and by controlling the RF amplitude of two frequency synthesizers. After an additional 0.1 ms, the synthesizer outputs are attenuated by RF switches. All of the other laser beams in this experiment are also gated using RF switches. Every critical laser beam also passes through a spatial filter to reduce scattered light when the RF switches are off—no mechanical shutters are used.

Launched atoms are subjected to a number of gated laser beams in the fountain. Even though the atoms are launched in the $6S$, $F = 4$ state, we first apply a repumping beam tuned to the $6S$, $F = 3 \rightarrow 6P_{3/2}$, $F = 4$ transition to ensure that essentially no atoms are in the $F = 3$ state. At 0.071 s after launching, a 0.75 G magnetic bias field is applied perpendicular to the plane of Fig. 1. At 0.109 s, we use a velocity-selective stimulated Raman transition to transfer atoms from the $6S$, $F = 4$, $m_F = 0$ state to the $6S$, $F = 3$, $m_F = 0$ state. The atoms are slowed by gravity and turn around approximately 5 cm above the photodiode in Fig. 1. As the atoms return to the detection chamber, at 0.278 s after launch, those that remain in the $F = 4$ state are "cleared" by absorbing $\approx$1000 photons from a circularly polarized laser beam tuned to the $6S$, $F = 4 \rightarrow 6P_{3/2}$, $F = 5$ transition. Another velocity-selective stimulated Raman transition probes the $6S$, $F = 3$, $m_F = 0$ state by transferring them to the $F = 4$, $m_F = 0$ state. This is followed at 0.292 s by a 0.8 ms pulse of a retroreflected "detection" laser beam tuned just below the $6S$, $F = 4 \rightarrow 6P_{3/2}$, $F = 5$ transition. A computer records the scattered light detected by the photodiode and amplifier.

To measure the temperature of the atoms, we scan the frequency of the first simulated Raman transition. The pulse sequence is the same as above except that we clear the remaining $F = 4$ atoms immediately after the first Raman pulse and then replace the second Raman pulse with a repumping pulse. In Fig. 2(a) curve (i) we show a frequency scan over the velocity distribution of the atoms in the $6S$, $F = 4$, $m_F = 0$ state. The data are the average of three frequency scans taken before and after the bulk of data reported here. The "Doppler shift" in Fig. 2(a) refers to the frequency difference of the two diode lasers used to drive the stimulated Raman transition. These lasers have a difference frequency of 9.2 GHz which is phase locked to a microwave oscillator and a tunable RF synthesizer. Also shown in Fig. 2(a) is a Gaussian fit corresponding to 1.53(7) μK. This is the lowest temperature reported for a six-beam molasses configuration and is significantly below the 2.5 μK minimum temperature measured by Salomon *et al.* [12]. Although our temperature is a factor of 2 higher than those recently demonstrated in an optical lattice [13], low lattice temperatures at the high atomic density needed for this experiment have not yet been reported.

The experiment to observe s-wave collisions is a variant of a pump-probe experiment. Here the pump is the first fixed frequency stimulated Raman pulse, which creates the narrow velocity distribution in the $F = 3$, $m_F = 0$ state, and the probe is the second stimulated Raman pulse which is frequency scanned. The desired signal occurs only when both pump and probe pulses are enabled. Therefore we take data by occasionally blocking the probe to measure the baseline offset with the pump enabled (signal) and disabled (background). It is also crucial to isolate the effects of collisions by measuring the response of the experiment in the absence of collisions. To do this, we enable the "clearing" beam immediately after the first stimulated Raman transition (pump) so that there is little time for collisions to occur. Again data are taken with the pump enabled and disabled so that data for a chosen v_z' consists of four interlaced scans: early and late clearing each with pump enabled and disabled. We also account for baseline drifts by measuring the difference of the digitized photodiode signal during the 0.8 ms detection pulse and immediately after it.

Data for selecting and probing are shown in Fig. 2(a) curve (ii). Here the pump was tuned to select atoms at $v_z' \approx 0$. The fluorescence versus probe frequency is essentially a Gaussian with a $1/e$ half-width of 4.872 kHz. While we can select narrower velocity slices, the selection width must be wide enough to obtain detectable signals, since the number of detected atoms that have undergone collisions is proportional to the width squared. Of course, resolution is lost if the selection is too wide. Further, it is advantageous for the selection wings go quickly to 0 to allow detection of collisions in many velocity classes. To do this, we use a Blackman stimulated Raman intensity pulse [14]. To reduce the background, the Raman lasers are tuned 3 GHz above the $D2$ transition to suppress spontaneous emission during the Raman pulses, which causes atoms to decay from the $6S$, $F = 4$ state to the $F = 3$ state and then back to $F = 4$. The peak height of the no-collision signal (ii) in Fig. 2(b) is 0.59 of the height of the thermal distribution (i). This is 84% of the 0.70 expected for the convolution of two Blackman pulses, indicating the Raman laser-beam intensities are reasonably uniform.

From the velocity distributions (iii) in Fig. 2(a), we see that collisions occur since fewer atoms remain at the

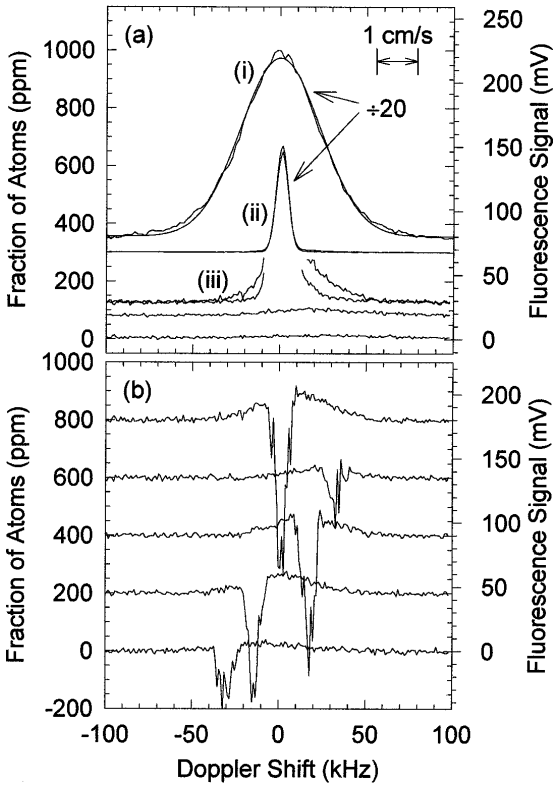

FIG. 2. (a) (i) Velocity distributions for $F = 4\, m_F = 0$ fountain atoms and a best fit corresponding to 1.53(7) μK. (ii) The no-collision signal [(early clearing,pump on) − (early,off)] and the collisions signal [(late,on) − (late,off)]—the difference in peak heights is 7.5%. (iii) Full size collision and no-collision signals. Note more atoms are detected in the collision signal at velocities different than the selected velocity. The bottom two curves are the backgrounds (late,off) and (early,off). (b) Difference of collision and no-collision velocity distributions for five v_z' spaced by 16 kHz or 6.8 mm/s. Approximately 7% of the atoms collide thereby appearing at $v_z \neq v_z'$ and disappearing from v_z'. The background noise is 5 ppm for one launch and the Doppler shift is measured relative to the center of (i).

selected velocity and an excess of atoms is detected at other velocities. In the Fig. 2(b) we show the difference of the collision and no-collision signals for several initial velocities v_z'. There is a noticeable asymmetry in most of these—this occurs because, when the selected atom has $v_z' \neq 0$, collisions on average restore a thermal distribution. An important contribution to these asymmetries is the two-photon recoils the atoms receive during a Raman transition [8]. In the uppermost scan, the asymmetry is entirely caused by the photon recoils, since the lasers were tuned to the peak of the thermal distribution. Twice the recoil velocity $h/m\lambda$ is 0.70 cm/s for $\lambda = 852$ nm which is nearly half of the most probable speed $u = 1.38$ cm/s.

One of the challenges of this experiment is to reduce the background noise so that it corresponds to several ppm of the total number of atoms. In Fig. 2(b), the background level is 200 ppm and the background noise is 5 ppm or 1.2 mV. The data in Fig. 2(b) are the average of four data sets. Since each set is an additive combination of the four scan types given by [(late clearing,pump on) − (late,off)] − [(early,on) − (early,off)], this noise level is also the background noise of a single launch. The noise is due to laser light scattered by the optics and the photodiode and amplifier noise. To achieve this background, it was necessary to eliminate the fluorescence background due to the tenuous room temperature "Cs beam" emitted from the vapor cell MOT. This was done by hyperfine pumping this atomic beam into the $6S$, $F = 3$ state using a laser beam tuned to the $6S$, $F = 4 \rightarrow 6P_{3/2}$, $F = 4$ transition. This laser beam passed through the center of the UHV MOT and was turned on 2 ms before the detection pulse.

Our signal-to-noise would improve if a lens or mirror imaged the fluorescence onto the 1 cm^2 photodiode. Unfortunately, imaging can distort the detected velocity distributions, since the position of a velocity class is correlated with its velocity. Therefore certain velocity classes could be preferentially imaged. Working with no imaging elements, we nonetheless test for preferential detection by checking if the areas of the measured difference velocity distributions are consistent with 0. We find no statistically significant areas suggesting homogeneous detection and a negligible number of inelastic collisions.

To determine whether the collisions we observe are s wave, we calculate difference velocity distributions that correspond to those in Fig. 2(b). The probability per unit time to go from v_z' to v_z is formally given by the velocity-changing collision kernel $W(v_z' \rightarrow v_z)dv_z$ [9,15]. However, a comparison of $W(v_z' \rightarrow v_z)$ and the data in Fig. 2(b) is not entirely meaningful because the fountain atoms spread during their flight so that collisions occurring late in the fountain trajectory have a lower collision energy. The importance of this is determined by the initial size of the laser-cooled sample and the velocity spread. We measure the density distribution of atoms at $t = 0.108$ s to be nearly Gaussian with a $1/e$ height of 0.64 cm. From this, our temperature measurement, and assuming the atom's initial position and velocity are uncorrelated Gaussian distributions, we infer an initial $1/e$ spherical radius of $r_0 = 0.283$ cm. Therefore the free flight expansion of the atoms causes the effective collision temperature to decrease as $T_{\mathrm{coll}}(t) = (1.53\ \mu\mathrm{K})/(1 + t^2/t_0^2)$, where $t_0 = r_0/u = 0.20$ s. In addition, dependent upon the v_z' we select, the atoms are detected at different positions and therefore collide with different density and velocity distributions. Accounting for these and the two-photon recoils the atoms receive at $t_1 = 0.109$ s, we calculate the velocity distribution due to collisions $N(v_z)$:

$$N(\nu_z) = \frac{1}{2} \int dz \int_{t_1}^{t_2} dt N_3 \frac{e^{-(z-\nu_z' t+\nu_{\mathrm{rec}} t_1)^2/r_0^2}}{r_0\sqrt{\pi}}\, n_4 \frac{e^{-z^2/r_0^2(1+t^2/t_0^2)}}{(1 + t^2/t_0^2)^{3/2}} W\left[\nu_z' - \nu_{z_0} \longrightarrow \nu_z - \nu_{z_0}; \frac{u}{\sqrt{1 + t^2/t_0^2}}\right] \Delta\nu_z\,.$$

Here N_3 is the number of selected $F = 3$, $m_F = 0$ atoms, $-v_{\rm rec}\hat{\mathbf{z}}$ is the two-photon recoil velocity, n_4 is the peak density at $t = 0$, $v_{z_0} = zt/(t^2 + t_0^2)$, and Δv_z is the detection bandwidth. To determine n_4, we use the total number of atoms and r_0 to infer $n_4 = 4.4 \times 10^{10}$ cm^{-3} to within a factor of 2 [16]. With this model, we calculate the velocity distributions shown in Fig. 3. For energy independent s-wave scattering, the cross section is 4×10^{-11} cm^2 and is the only parameter in the fit. In Fig. 3 we do not show the loss of atoms from v_z' for clarity.

In Fig. 3 we also show a best fit of the velocity distribution to a p-wave differential cross section $d\sigma/d\Omega(\theta, v_r) \propto \cos^2(\theta) v_r^4$. We choose a v_r^4 dependence because the p-wave scattering cross section should scale as T^2 at low energy. While a small p-wave contribution is expected, if it were dominant a simple $\cos^2(\theta)$ differential cross section for elastic collisions would not be expected. This is because the 0.75 G magnetic bias field will cause the electron spins to precess about the magnetic field which will, in general, change the projection on the collision axis. However, it can be seen in Fig. 3 that, when $|v_z'| \gtrsim u$, the difference between $\cos^2(\theta)$ and isotropic s-wave scattering are more pronounced than for $v_z' = 0$. When $v_z' \gg u$, the collision axis is oriented along the magnetic field direction so that a $\cos^2(\theta)$ distribution is expected.

At low temperatures s-wave scattering should dominate. Although the total cross section is simply the sum of the p-wave and s-wave total cross sections, the angular distribution of the scattering has an important interference term. Our data are more sensitive to interference terms as compared to whether the scattering is s, p, or d wave. For example, the difference between pure p-wave and pure s-wave scattering is an excess of scattering around $\theta = 90°$. Adding a small p-wave component gives a differential cross section $d\sigma/d\Omega = a^2 + 2ab\cos(\phi)\cos(\theta) + b^2\cos^2(\theta)$, where ϕ is the relative phase shift. Here, the effect is to create a difference between forward ($\theta = 0$) and backward scattering ($\theta = 180°$) to which the velocity distributions are more sensitive. To illustrate, in Fig. 3 we also show the velocity distribution for an admixture of 90% s wave and 10% p wave for $\phi = \pi$. From a χ^2 fit, the ratio of p-wave to s-wave cross sections is $1.2(1.0) \times 10^{-3}$ for $\phi = \pi$. For an incoherent sum of s-wave and p-scatterings (or $\phi = \pm\pi/2$), we get a p-wave fraction of 0.01(3). From these we conclude the collisions we observe are almost entirely s wave.

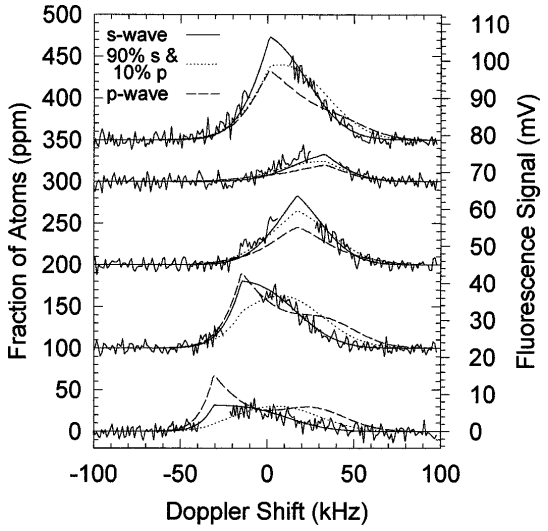

FIG. 3. Data and calculated velocity distributions. Solid lines are the data and the calculated velocity distributions for an s-wave cross section of 4×10^{-11} cm^2. Also shown are the velocity distributions for pure p-wave scattering (dashed) and an admixture of 90% s-wave and 10% p wave with a relative phase shift of $\phi = \pi$ (dotted).

We acknowledge discussions with Boudewijn Verhaar and support from a NIST Precision Measurement grant, a NSF NYI award, and Yale University. One of us (R. L.) acknowledges support under a NSF Graduate Research Fellowship.

[1] See J. P. Bouchaud and C. Lhuillier, J. Phys. **46**, 1101 (1985); P. S. Julienne and F. H. Mies, J. Opt. Soc. Am. B **6**, 2257 (1989).
[2] N. Masuhara *et al.*, Phys. Rev. Lett. **61**, 935 (1988); C. R. Monroe *et al., ibid.* **70**, 414 (1993); W. Petrich *et al., ibid.* **74**, 3352 (1995); N. R. Newbury, C. J. Myatt, and C. E. Wieman, Phys. Rev. A **51**, 2680 (1995); C. S. Adams *et al.*, Phys. Rev. Lett. **74**, 3577 (1995); K. B. Davis *et al., ibid.* **74**, 5202 (1995); M. H. Anderson *et al.*, Science **269**, 198 (1995).
[3] E. Tiesinga *et al.*, Bragt, Phys. Rev. A **45** (1992).
[4] M. Bijlsma, B. J. Verhaar, and D. J. Heinzen, Phys. Rev. A **49**, 4285 (1994).
[5] K. Gibble and S. Chu, Phys. Rev. Lett. **70**, 1771 (1993).
[6] E. S. Meyer, J. C. Mester, and I. F. Silvera, Phys. Rev. Lett. **70**, 908 (1993); J. C. Mester *et al., ibid.* **71**, 1343 (1993).
[7] W. N. Hardy *et al.*, Phys. Rev. Lett. **45**, 453 (1980); M. Morrow *et al., ibid.* **46**, 195 (1981); M. E. Hayden, M. D. Hurlimann, and W. N. Hardy, IEEE Trans. Instr. Meas. **42**, 314 (1993).
[8] M. Kasevich *et al.*, Phys. Rev. Lett. **66**, 2297 (1991).
[9] See P. R. Berman, Phys. Rev. A **5**, 927 (1972); P. F. Liao, J. E. Bjorkholm, and P. R. Berman, *ibid.* **21**, 1927 (1980).
[10] C. Monroe *et al.*, Phys. Rev. Lett. **65**, 1571 (1990); K. E. Gibble, S. Kasapi, and S. Chu, Opt. Lett. **17**, 526 (1992).
[11] For a magnetic trap, see E. A. Cornell, C. R. Monroe, and C. E. Wieman, Phys. Rev. Lett. **67**, 2439 (1991).
[12] C. Salomon *et al.*, Europhys. Lett. **12**, 683 (1990).
[13] A. Kastberg *et al.*, Phys. Rev. Lett. **74**, 1542 (1995).
[14] M. Kasevich and S. Chu, Phys. Rev. Lett. **69**, 1741 (1992).
[15] See P. R. Berman, T. W. Mossberg, and S. R. Hartmann, Phys. Rev. A **25**, 2550 (1982).
[16] The $m_F = 0$ fraction is $\approx \frac{1}{11}$. The $m_F < 0$ states have as much as twice the population as the $m_F > 0$ states.
[17] A Cu gasket forms the UHV seal; A. Noble and M. Kasevich, Rev. Sci. Instrum. **65**, 3042 (1994).